A functional study of plasma-membrane calcium-pump isoform 2 mutants causing digenic deafness

R. Ficarella*, F. Di Leva†, M. Bortolozzi‡, S. Ortolano‡, F. Donaudy*, M. Petrillo*, S. Melchionda§, A. Lelli‡, T. Domi†, L. Fedrizzi†, D. Lim‡, G. E. Shull¶, P. Gasparini*∥, M. Brini†**, F. Mammano‡**††, and E. Carafoli‡**

*Telethon Institute of Genetics and Medicine, 80131 Naples, Italy; Departments of †Biochemistry, Experimental Veterinary Sciences, and ††Physics, University of Padua, 35121 Padua, Italy; ‡Venetian Institute of Molecular Medicine, 35129 Padua, Italy; §Unit of Medical Genetics, Instituto di Ricovero e Cura a Carattere Scientifico, Casa Sollievo della Sofferenza, 71013 San Giovanni Rotondo, Italy; ¶Department of Molecular Genetics, University of Cincinnati, Cincinnati, OH 45221; and ∥Unit of Medical Genetics, Department of Reproductive Science and Development, Instituto di Ricovero e Cura a Carattere Scientifico-Burlo Garofalo, University of Trieste, 34127 Trieste, Italy

Ca^{2+} enters the stereocilia of hair cells through mechanoelectrical transduction channels opened by the deflection of the hair bundle and is exported back to endolymph by an unusual splicing isoform (w/a) of plasma-membrane calcium-pump isoform 2 (PMCA2). Ablation or missense mutations of the pump cause deafness, as described for the G283S mutation in the deafwaddler (dfw) mouse. A deafness-inducing missense mutation of PMCA2 (G293S) has been identified in a human family. The family also was screened for mutations in cadherin 23, which accentuated hearing loss in a previously described human family with a PMCA2 mutation. A T1999S substitution was detected in the cadherin 23 gene of the healthy father and affected son but not in that of the unaffected mother, who presented instead the PMCA2 mutation. The w/a isoform was overexpressed in CHO cells. At variance with the other PMCA2 isoforms, it became activated only marginally when exposed to a Ca^{2+} pulse. The G293S and G283S mutations delayed the dissipation of Ca^{2+} transients induced in CHO cells by $InsP_3$. In organotypic cultures, Ca^{2+} imaging of vestibular hair cells showed that the dissipation of stereociliary Ca^{2+} transients induced by Ca^{2+} uncaging was compromised in the dfw and PMCA2 knockout mice, as was the sensitivity of the mechanoelectrical transduction channels to hair bundle displacement in cochlear hair cells.

hereditary hearing loss | mutations | calcium homeostasis | calcium transport

The receptive organelle of sensory hair cells in the mammalian cochlea, the stereocilia bundle, protrudes from the cell's apical surface. Inner hair cells transduce mechanical vibrations into electrical signals that are eventually transmitted to the brain to be transformed into hearing signals (1), whereas outer hair cells (OHCs) (2) amplify the vibrations of the basilar membrane (3). Mechanical stimuli that are detected as excitatory deflect a hair bundle, thus increasing tension in the tip link, a filament stretched between the tops of stereocilia. This tension is conveyed to mechanosensitive transduction (MET) channels that open to allow ions into the cell (4). The apical surface of hair cells is bathed in endolymph, which is rich in K^+ but low in Na^+ and Ca^{2+} (5). K^+ carries most the transduction current, but MET channels are Ca^{2+} selective, i.e., Ca^{2+} influx is significant even at the low Ca^{2+} levels of the endolymph (6–10): 20–23 μM in the rodent cochlea (11, 12), 200–250 μM in the vestibular system, possibly because of the presence there of calcium carbonate crystals (13, 14). Approximately 10% of the MET current may actually be carried by Ca^{2+} ions (15). Ca^{2+} entering through MET channels is rapidly sequestered by buffers in the stereocilia (16, 17) and is shuttled back to endolymph by the plasma membrane Ca^{2+} pump (PMCA) (18, 19), which is very concentrated in the stereocilia membrane ($\approx$2,000 per squared micrometer) (15, 19–21). The PMCA is assumed to increase Ca^{2+} in the immediate proximity of the hair bundle (19), possibly with the complicity of the acellular structures overlying the hair cells in the cochlea (22) and, particularly, in the vestibular system (14), where the pump also would contribute to the formation and maintenance of the otoconia (23).

Of the four basic isoforms of the PMCA pump,‡‡ two (PMCA1 and PMCA4) operate in all tissues and two (PMCA2 and PCMA3) operate in specialized tissues, such as muscle and, especially, brain (24, 25). All four isoforms display splice variants caused by the insertion of alternative exons at site A in the cytosolic loop connecting transmembrane domains 2 and 3 and at site C in the C-terminal tail of the pump. Alternative splicing is peculiarly complex in PMCA2 because it involves the insertion of up to three novel exons at site A and of two at site C. The A-site insertions are in-frame, creating variant w when three exons are inserted (the normal variant without site-A inserts is termed z). The insert at site C creates instead a novel stop codon, leading to the truncation of the pump (variants a and b being the normal full-length pump). The site-C insertions eliminate approximately half of the calmodulin binding domain; those at site A occur next to a domain that binds activatory acidic phospholipids, which, however, also bind to the calmodulin binding domain (26). As expected, the site-C insertions lower the affinity of PMCA pumps for calmodulin (27) but do not compromise the activation by acidic phospholipids, which is alternative to that by calmodulin (28). The site-A insertion, in contrast, could impair the activation by acidic phospholipids, particularly in the C-terminally truncated pump variants, in which the C-terminal phospholipid binding domain also is compromised.

Several splice variants of the four PMCAs have been detected in cochlear cDNAs (29), the C-terminally truncated PMCA2a being the only isoform detected in the stereocilia of hair cells (30). PMCA1b prevails instead in basolateral membranes. Recent work has shown that the truncated isoform in the stereocilia of OHCs is also spliced at site A and is thus the w/a variant (31). It is plausible
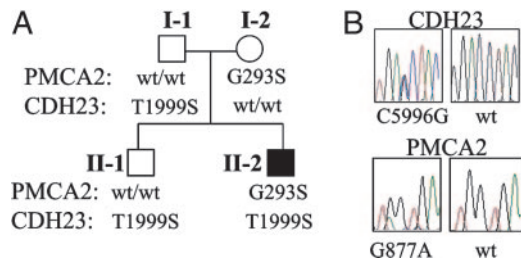
Fig. 1. Association of digenic mutations of PMCA2 and CDH23 with hearing loss. (*A*) Pedigree of an Italian family. Black symbols denote the family members affected. Genotypes of PMCA2 and CDH23 are indicated for each individual. (*B*) Representative chromatogram of CDH23 C5996G and PMCA2 G877A, respectively, which were identified from the family.

to assume that the choice of this unusual variant of the PMCA (32) was dictated by the special Ca^{2+} homeostasis demands of the ambient in which the pump must operate.

Mutations of PMCA2 have been recently shown to induce recessively inherited deafness (33). A G283S mutation replaced a conserved G [supporting information (SI) Fig. 5] downstream of the phospholipids binding domain of the pump (deafwaddler mouse, *dfw*). A mutation next to the active center (V586M) was later found to depress pump activity and to increase hearing loss in heterozygous patients that also carried a homozygous mutation in cadherin 23 (CDH23) (34). A mutation has now been identified in the human PMCA2 gene that replaces a conserved glycine residue (G293S) 10 residues downstream of the *dfw* mutation.

For the present work, the activity of the recombinant *w/a* variant of the PMCA2 pump was compared in the natural environment of model cells with the other variants of the pump and with the *dfw* pump and the pump carrying the G293S mutation. The *dfw* pump also has been studied biochemically and electrophysiologically in organotypic cultures of mice cochleae and utricles, and the results have been compared with those in WT mice and in mice in which the PMCA2 gene had been ablated (23).

Results

Genetic Analysis of the PMCA2 Mutation. A mutational screening of the PMCA2 gene (GenBank accession no. NM_001001331.1) on samples of 450 subjects coming from different countries identified a missense mutation associated with autosomal dominant hearing loss. The mutated allele was a G→A transition at position 877 in exon 5 of the nucleotide sequence, leading to the replacement of a highly conserved glycine with a serine at position 293 in the cytosolic loop connecting transmembrane domains 2 and 3 (the region in which the mutation G283S of *dfw* maps). The mutated allele was detected in an Italian patient affected by severe bilateral sensorineural hearing impairment without vestibular involvement. Two hundred chromosomes of individuals coming from the same geographical area of the patient were negative for the presence of the mutated allele. The G293S mutation was inherited from the mother who had normal hearing. The father and a brother of the patient, with normal hearing, were negative for the G293S mutation. Considering the recent finding of a contribution of the PMCA2 gene mutation as a modifier of the hearing loss phenotype (34), the whole family was analyzed for the presence of mutations in other genes that are also frequently involved in hereditary hearing loss: connexin 30 (GJB6), myosin 6 (MYO6), and CDH23; mitochondrial DNA was also screened. The screening on the CDH23 gene (GenBank accession no. NM_022124.2) has identified a T→S substitution at position 1999 (C5996G) in the affected son but not in the mother (Fig. 1). This mutated allele, which had already been described in a mutation database as a polymorphism, was inherited by the patient from his healthy father and also was
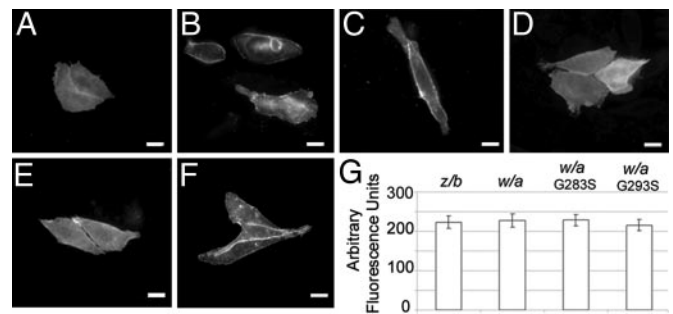

Fig. 2. Immunolocalization of recombinant PMCA2 variants and mutants in transiently transfected CHO cells. (*A–D*) PMCA2 variants *w/b* (*A*), *z/a* (*B*), *z/b* (*C*), and *w/a* (*D*). The interaction with antibody 5F10 was revealed by the Alexa Fluor 488-conjugated secondary antibody. (*E* and *F*) PMCA mutants on the *w/a* construct G283S (*E*) and G293S (*F*) were stained with antibody 2N, and the interaction was visualized by the Alexa Fluor 488-conjugated secondary antibody. The plasma membrane pattern of the overexpressed proteins in representative cells is shown. (*G*) The level of fluorescence in the plasma membrane was quantified as described in *Materials and Methods*. The SDs are indicated by the bars. Immunocytochemistry was performed as described in *Materials and Methods*. (Scale bars, 20 μm.)

present in the healthy brother (Fig. 1). Negative results were obtained for the other DNA sequences analyzed.

Comparative Analysis of the Ca^{2+} Handling Activity of the Splice Variants of PMCA2 and of the Mice and Human Mutants. Mammalian expression plasmids for the *dfw* (G283S) and human (G293S) *w/a* mutants were generated and transfected in CHO cells. Expression plasmids were also prepared for the other PMCA2 splice isoforms *z/b*, *z/a*, *w/b*. Appropriate controls (Western blots and quantitative immunocytochemistry) established that all variants of the pump were expressed at equivalent levels and were correctly delivered to the plasma membrane (Fig. 2 and SI Fig. 6). The transfection routinely yielded 10–15% positive cells, of which 50% had a pure plasma-membrane targeting pattern, i.e., a clear signal at the cell surface (on which quantitative immunofluorescence was performed). In the remainder of the cell population both rim staining and endoplasmic reticulum expression patterns were visible. Because the PMCA units retained in the endoplasmic reticulum are normally inactive (35), they do not influence Ca^{2+} homeostasis. The percentage of cells with unambiguous plasma membrane pattern was obtained by counting hundreds of cells for each transfection experiment. CHO cells were cotransfected with the Ca^{2+}-sensitive photoprotein aequorin (36) and stimulated with ATP, an $InsP_3$-linked agonist that acts on P2Y purinergic receptors. Under the experimented conditions, the height of the Ca^{2+} transient generated by the opening of the $InsP_3$ receptor was controlled primarily by the PMCA pumps, not by the SERCA pump. In some experiments, the latter was silenced with the specific inhibitor 2,5-di-*tert*-butyl-1,4 benzohydroquinone, with marginal changes in the height of the Ca^{2+} peak and in the kinetics of the return of the traces to baseline. Evidently, the activity and/or amount of overexpressed PMCA pump overshadowed those of the native SERCA pump. The postpeak decay kinetics of the traces is expected to be influenced by Ca^{2+} influx through store-operated Ca channels. No efforts were made to eliminate their contribution to the shape of the Ca^{2+} curves because it was felt that the effects would have been the same for all pump variants.

The overexpression of the four splice variants of the pump affected the ability of the cells to handle Ca^{2+} (Fig. 3*A*). The lowering of the Ca^{2+} peak with respect to untransfected cells reflects the ability of the pump to respond with a burst of activation to the sudden arrival of a Ca^{2+} pulse. Two of the splice variants (*z/a* and *w/b*) had essentially the same effect on the Ca^{2+} peak of the
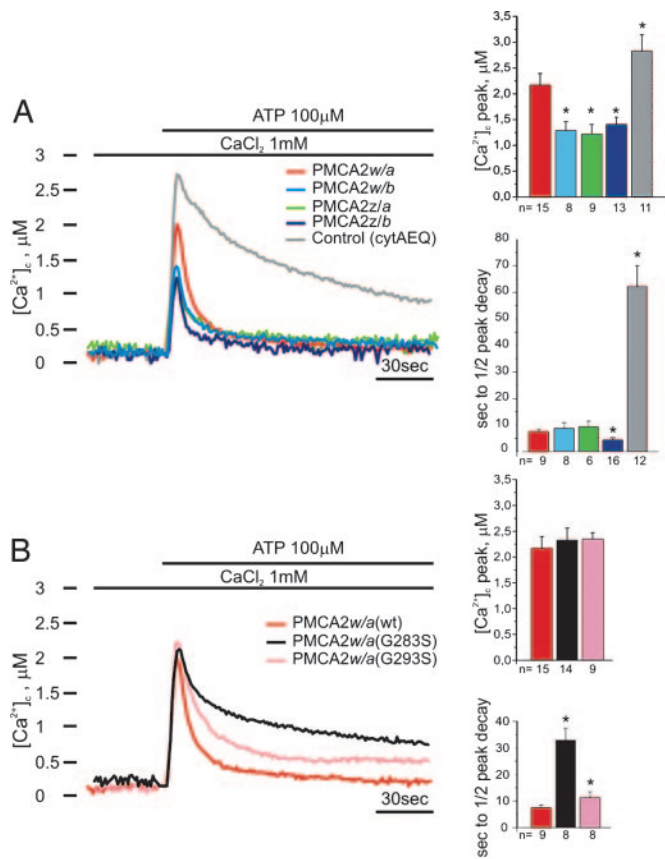
BIOCHEMISTRY

Fig. 3. Activity of recombinant PMCA2 isoforms (*A*) and of the mutated *w/a* isoforms (*B*) in CHO cells. CHO cells were transiently cotransfected with the PMCA2 variants and cytAEQ or with only cytAEQ (as a control). The cells were then perfused with KRB supplemented with $CaCl_2$ (1 mM). We used 100 μM ATP to produce a transient increase of $[Ca^{2+}]_c$. The histograms show the means ± SD of $[Ca^{2+}]_c$ peaks and of the half-peak decay times. The traces are representative of at least eight experiments. *, $P < 0.01$ calculated with respect to PMCA2*w/a*.

full-length, nonspliced PMCA2*z/b*, which is a very active PMCA isoform (32) (see histograms on $[Ca^{2+}]_c$ peak in Fig. 3*A*). By contrast, the doubly spliced variant *w/a* was less able to control the peak height; i.e., it reacted less to the incoming Ca^{2+} pulse. However, when the function of the pump became the longer-term control of postpeak Ca^{2+}, i.e., when only nonactivated pumping was presumably required, all variants, including the *w/a*, became equivalent (the *z/b* was slightly more efficient; see histograms on half peak decay time in Fig. 3*A*). Fig. 3*B* shows the same type of experiment on the *dfw* (G283S) and human mutants (G293S), which were expressed in amounts equivalent to those of the other isoforms, and were correctly sorted to the plasma membrane (Fig. 2 and SI Fig. 6). The two mutant pumps were as ineffective as the WT *w/a* in lowering the Ca^{2+} peak (2.2 ± 0.2 μM, $n = 15$ for *w/a*; 2.3 ± 0.2 μM, $n = 14$ for *w/a* G283S; and 2.3 ± 0.1 μM, $n = 9$ for *w/a* G293S). Instead, the declining phase of the Ca^{2+} curve was much slower in the mutant pumps than in the WT *w/a* variant (half peak decay time: 32.9 ± 4.4 s, $n = 8$ for *w/a* G283S; 11.3 ± 2.3 s, $n = 8$ for *w/a* G293S; and 7.4 ± 1.0 s, $n = 9$ for the WT *w/a*). The defect was more pronounced in the *dfw* mutant than in the G293S mutant. The increased severity of the *dfw* mutation was made more evident when the mutations were introduced in the full-length PMCA2 variant (*z/b*). The Ca^{2+} handling defect became even more dramatic in the *dfw* mutant but was less evident in the G293S human mutation (see SI Fig. 7).
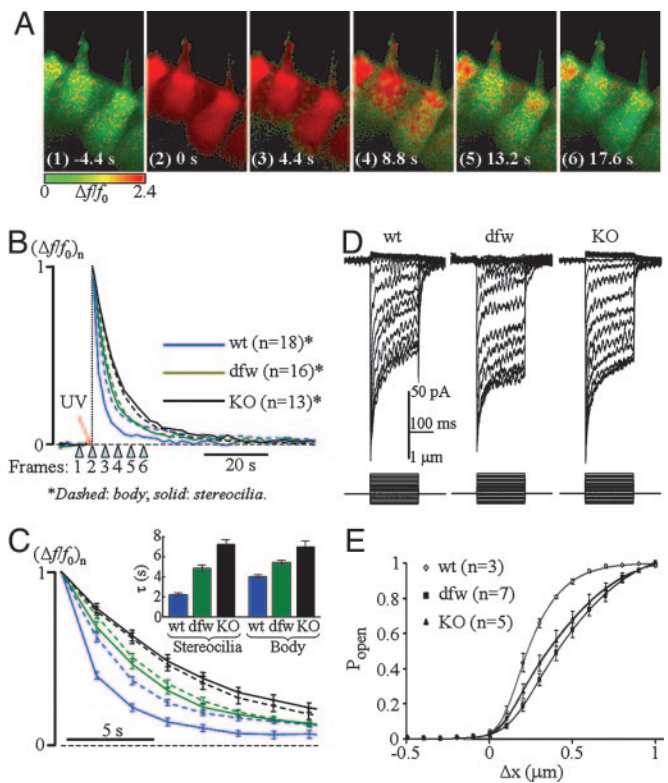

Fig. 4. Ca^{2+} extrusion and MET currents in hair cells of PMCA2 KO and *dfw* mice. (*A*) Time sequence of confocal images before and after UV photolysis of caged calcium in hair cells of an utricle culture (P2) from PMCA2 KO mice. Timing relative to the onset of the 100-ms UV light (375 nm) delivery is shown on each numbered frame. The example of Ca^{2+} concentration change was probed by the $\Delta f/f_0$ signal encoded by the color scale bar beneath frame 1. (*B*) Time course of normalized fluorescence ratio changes ($\Delta f/f_0$)$_n$ evoked by Ca^{2+} photoliberation. Each data point is averaged over $n > 13$ cells in two to four mice of each type, encoded by colored lines (solid lines, stereocilia; dashed lines, cell body excluding stereocilia) for WT controls (wt, blue traces), *dfw* (green traces), and PMCA2 KO (black traces) mice. The arrowheads below the time axis show the time of frame capture from *A*. (*C*) Same as *B* for the first 15 s after UV application. (*Inset*) Decay time constants τ were derived by a single-exponential fit. The ANOVA test gave $P < 10^{-4}$ and $P = 0.03$ for compatibility of stereociliary τ of WT *dfw* and *dfw* KO, respectively. (*D*) MET currents in OHCs for displacements of the tip of the hair bundle toward or away from the kinocilium. In the stimulus monitor shown at the bottom, positive steps indicate (excitatory) movements toward the highest stereocilia. Inward currents are given as negative relative to the current level in the absence of bundle stimulation at the holding potential, −80 mV. The high-frequency oscillations in the current traces were due to imperfectly cancelled environmental mechanical disturbances. Each response is the average of 10 presentations. (*E*) Plots of peak MET current versus displacement, Δx, of the tip of the hair bundle. Peak current was measured from records like those in *D* expressed as the difference in current relative to that obtained with a large negative displacement, where all transducer channels are assumed to be closed, and peak current was normalized to yield a measure of channel open probability (P_{open}, ordinates). Smooth curves are least-square fits calculated from $P_{open} = 1/(1 + e^{A2(X2 - \Delta x)} \cdot (1 + e^{A1(X1 - \Delta x)}))$, where A_1, A_2, X_1, and X_2 are fit parameters. For WT, $A_1 = 13.91 ± 2.35$ μm^{-1}, $A_2 = 7.17 ± 0.77$ μm^{-1}, $X_1 = 0.14 ± 0.03$ μm, and $X_2 = 0.20 ± 0.02$ μm; for *dfw*, $A_1 = 9.85 ± 1.15$ μm^{-1}, $A_2 = 3.99 ± 0.43$ μm^{-1}, $X_1 = 0.21 ± 0.03$ μm, and $X_2 = 0.43 ± 0.01$ μm; and for KO, $A_1 = 13.79 ± 1.09$ μm^{-1}, $A_2 = 4.34 ± 0.19$ μm^{-1}, $X_1 = 0.14 ± 0.01$ μm, and $X_2 = 0.37 ± 0.01$ μm.

Ca^{2+} Homeostasis in the Hair Cells of Cultured Utricles of WT, PMCA2 Knockout (KO), and *dfw* Mice. To investigate pump activity *in situ*, confocal fluorescence imaging was performed on utricle organotypic cultures obtained from postnatal day P0 to P3 mice, observed between P1 and P4. Cultures were coloaded with the single

Table 1. Clearance rate of Ca^{2+} in stereocilia and body of OHCs in WT, *dfw*, and PMCA2 KO mice

Variable	Mouse	Stereocilia	Body
τ, s	WT	2.2 ± 0.2 ($n = 18$)	4.0 ± 0.3
	dfw	4.8 ± 0.6 ($n = 16$)	5.4 ± 0.3
	KO	7.2 ± 0.8 ($n = 13$)	7 ± 1
$(\Delta f/f_0)_{peak}$	WT	1.7 ± 0.2 ($n = 18$)	3 ± 0.3
	dfw	3.5 ± 0.6 ($n = 16$)	4 ± 0.4
	KO	2 ± 0.4 ($n = 13$)	2.3 ± 0.5

Data are shown as means $\pm$ SEM. The age of each mouse was between P1 and P4.

wavelength indicator fluo-4 and with *o*-nitrophenyl-EGTA, which released caged Ca^{2+} upon UV light illumination. After obtaining a reading for the baseline fluorescence of the indicator, UV exposure generated a uniform Ca^{2+} transient distributed over the whole cell, which was quantified as $\Delta f/f_0 = (f - f_0)/f_0$, where f is fluorescence at time t and f_0 is prestimulus fluorescence (Fig. 4*A*). In WT mice, the recovery to baseline Ca^{2+} was slightly but significantly ($P < 10^{-4}$) faster in the stereocilia (time constant $\tau = 2.2 \pm 0.2$ s, $n = 18$) than in the corresponding cell body ($\tau = 4.0 \pm 0.3$ s, $n = 18$) (Fig. 4 *B* and *C*, solid and dashed lines for stereocilia and cell body, respectively). This result shows that stereocilia are Ca^{2+} microdomains (17) in which Ca^{2+} gradients generated during mechanotransduction (9) are dissipated independently from the cell body (18). τ was significantly larger in *dfw* than in WT and, particularly, in PMCA2 KO mice. The results in Fig. 4*C Inset* and Table 1 show that ablation of PMCA2, or impairment of its activity, decreased the Ca^{2+} clearing rate of the stereocilia, making it similar to the slower rate of cell soma.

MET Currents in OHCs of WT, PMCA2 KO, and *dfw* Mice. Hair cells detect vibrations of atomic dimensions of the order of 0.2 nm (37) [in the mouse cochlea, their operating range is ≈ 500 nm (38)]. To assay transduction, organotypic cochlear cultures from P0–P3 mice were studied between P1 and P4 (for details, see *Materials and Methods*). The amplitude and kinetics of the currents in PMCA2 KO and *dfw* mice were qualitatively similar to those of WT controls (Fig. 4*D*). However, the curves relating bundle displacement (X) to channel opening probability, P_{open} (X), in *dfw* and PMCA2 KO mice were shifted positively with respect to controls (Fig. 4*E*). The shift was more pronounced in the KO mice (175 nm) than in the *dfw* mice (117 nm). These results are consistent with those obtained with vanadate, which blocks Ca^{2+} extrusion in auditory hair cells (39) and induces a similar (≈ 200 nm) shift in the P_{open} (X) curve (40).

Discussion

A number of genes and proteins have been associated with hereditary hearing loss, the most common sensory deficit in humans (41). As discussed in the Introduction, a recent addition to the list is *Atpb2*, encoding the PMCA2 pump, which is specifically expressed in the stereocilia of hair cells. Isoform 2 of the PMCA pump has properties that distinguish it from other PMCA isoforms: When tested in the cellular environment, it is two to three times more active than the two ubiquitous pumps in pumping Ca^{2+} out of the cell (32). In the isolated state, it shows very high calmodulin affinity (K_d, 2–4 nM) (27); i.e., it becomes fully activated under conditions (e.g., calmodulin and/or Ca^{2+} concentration) that would very poorly activate isoforms 1 and 4. PMCA2 also has peculiarly high activity in the absence of activators (42). But the property that distinguishes PMCA2 most clearly is the complexity of alternative splicing. The stereocilia of the OHCs contain a splice variant (*w/a*) that has high basal Ca^{2+} ejection activity but fails to respond with rapid activation to the sudden arrival of a Ca^{2+} load. As mentioned above, these properties evidently satisfy the Ca^{2+} homeostasis demands of the endolymph and of the stereocilia. Even if Ca^{2+} in the endolymph is very low, the recently measured value of 23 μM (12) is considerably higher than that necessary for the integrity of the tip links, which is compromised only below 1 μM Ca^{2+} (43). In fact, even the inactivating *dfw* mutation lowers the endolymph Ca^{2+} concentration only to ≈ 6 μM (12). However, a number of *in vitro* studies have shown that the generation of MET currents, for instance, in chickens, requires a minimum of 20 μM extracellular Ca^{2+} and is not elicited at 10 μM (7). Other studies have shown that MET currents require a minimum of 10 μM external Ca^{2+} in bullfrog (6), and adaptation, the process by which hair cells continuously readjust their sensitivity to the ciliary bundle displacements (44, 45), is slowed when extracellular Ca^{2+} is reduced (15, 19, 46, 47).

Within the stereocilia, the control of Ca^{2+} is vital to a number of aspects of the mechanotransduction process, e.g., the regulation of adaptation (44, 45), the ability to sense the deflection of the ciliary bundle with high sensitivity (37), and the breaking and regeneration of tip links (48). As mentioned above, these peculiar functions of the Ca^{2+} signal have in all likelihood dictated the choice of the PMCA2*w/a* isoform. Because resting stereociliary Ca^{2+} is very low (9, 18), it makes sense to control it with a pump variant that decreases Ca^{2+} to lower concentrations than other isoforms (27), even if it is insensitive to calmodulin (and, presumably, to acidic phospholipids). The relative insensitivity of the *w/a* pump to calmodulin makes good sense, given that its very high concentration in the stereocilia (70 μM) (49) would produce permanent maximal activation of pump isoforms normally sensitive to it. A comment would also be in order on CDH23, which binds harmonin, an F-actin bundling protein that may anchor it to the actin core of the stereocilia (50). Harmonin also binds myosin VIIa, suggesting a role for the complex harmonin–myosin VIIa, CDH23, in the cohesion of the stereocilia (50). Whether the tripolar complex has any role in the function of PMCA2 is an open question.

The study has shown that the function compromised in the mutated pumps is not the ability to respond to a sudden demand of hyperactivity, which is about the same in the WT *w/a* variant, but the special ability to operate efficiently at the nonactivated level. The mutations impair the longer-term export of Ca^{2+}, in agreement with the measurements of endolymphatic Ca^{2+} levels in the *dfw* mouse model (12), but endolymphatic Ca^{2+} also influences stereociliary Ca^{2+}. By controlling the multiple phases of adaptation, Ca^{2+} influx contributes to setting the resting position of the hair bundle and thus influences the fraction of MET channels open at rest. By increasing Ca^{2+} near the stereocilia tips, the pump augments the probability of blocking MET channels and increases the rate of adaptation. Conversely, lowering Ca^{2+} would reduce the rate of adaptation and increase open probability and channel unitary conductance (51). Even if the low Ca^{2+} levels in *dfw* endolymph preserve tip links (43), under these conditions MET channels will become biased toward the full open state. OHCs containing mutated pumps would therefore become insensitive to bundle displacements, and MET currents would be replaced by a large standing current that would permanently depolarize the cells' state. Eventually, Ca^{2+} loading via voltage-gated channels in the basolateral membrane and/or excitotoxic effects would doom OHCs. In the vestibular system, the cell fate may be delayed, albeit only temporarily, by the Ca^{2+} buffering action of the otoconia.

Materials and Methods

Genetic Analysis of Human PMCA Mutations. More than 400 subjects were analyzed for mutations in the PMCA2*a* gene. The inclusion criteria were (*i*) absence of the most common mutations within the GJB2 gene, (*ii*) sensorineural hearing loss, and (*iii*) normal tympanometric evaluation. In all cases, vestibular data were obtained by clinical examination and routine vestibular tests (one or more of the following: caloric, rotatory, optokinetic, swinging torsion, statokinesimetric, and vestibulo-vegetative). The series includes cases

BIOCHEMISTRY

with a variable degree of hearing loss, ranging from mild to profound and with age onset varying from congenital to late onset. Familial records were available in most cases. The majority of patients came from Central and Southern Italy (200), 140 were from Spain, and 54 were from Belgium. After informed consent, peripheral blood was obtained, and DNA was isolated from blood leukocytes according to standard methods. Fifty primer pairs were designed to amplify the 22 coding exons of the PMCA2 gene, including the splice sites and 5′ UTR and 3′ UTR regions. Moreover, 128 primer pairs were designed to amplify 67 coding exons, including the splice site of the CDH23 gene (PCR primer sequences and conditions are available upon request). All amplicons were screened by denaturing HPLC on a WAVE Nucleic Acid Fragment Analysis System HSM (Transgenomic, Omaha, NE) according to the supplier's protocols. Denaturing HPLC data analysis was based on a subjective comparison of sample and reference chromatograms. PCR products showing an abnormal chromatographic profile were directly sequenced on an automated sequencer (ABI 3100; Perkin–Elmer, Wellesley, MA).

Cloning and Expression of PMCA2 Isoforms and of Mutants G283S and G293S. Site-directed mutagenesis was carried out to obtain mutants cloned in the appropriate vector. Both PMCA2w/a and PMCA2z/b were used as targets, and experiments were performed according to the manufacturer's standard protocol (Stratagene, Cedar Creek, TX). The following primers were used: G283S, tgaactctcagactagcatcatctttacc (forward) and ggtaaagatgatgctagtctgagagttca (reverse); G293S, cctcctgggggctggtagtgaagaggaagagaa (forward) and ttctcttcctcttcactaccagccccaggagg (reverse).

Immunolocalization of the Expressed Pumps. CHO cells were grown in Ham's F12 medium supplemented with 10% FCS. Before transfection, the cells were seeded onto 13-mm glass coverslips and allowed to grow to 50% of confluence. Transfection with 3 μg of plasmid DNA (or 1.5:1.5 μg in the case of cotransfection) was carried out with a Ca-phosphate procedure (52).

Thirty-six hours after transfection, CHO cells were processed for immunofluorescence. The cells were washed twice with PBS (140 mM NaCl/2 mM KCl/1.5 mM KH$_2$PO$_4$/8 mM Na$_2$HPO$_4$, pH 7.4), fixed for 20 min in 3.7% formaldehyde, washed three times with PBS, and then incubated for 10 min in PBS supplemented with 50 mM NH$_4$Cl. The cells were then permeabilized in 0.1% Triton X-100 in PBS, followed by a 1-h wash with 1% gelatin (type IV, from calf skin) in PBS. Cells were then incubated for 1 h at 37°C in a wet chamber with polyclonal isoform-specific PMCA antibody 2N (Affinity BioReagents, Golden, CO) or a monoclonal antibody recognizing all pump isoforms (5F10; Affinity BioReagents) at a 1:100 dilution in PBS. Staining was carried out with Alexa Fluor 488-labeled anti-rabbit or anti-mouse secondary antibodies (Molecular Probes, Carlsbad, CA) at a 1:50 dilution in PBS. After each incubation, cells were washed four times with PBS. Fluorescence was analyzed with an Axiovert microscope (Zeiss, Oberkochen, Germany) equipped with an AxioCam HRm camera (Zeiss). Images were acquired with AxioVision vs30 software (Zeiss).

Membrane Fluorescence Computation. Immunocytochemistry was performed to quantify the expressed pump proteins in the plasma membrane of transfected cells. CHO cells transfected with the constructs expressing the PMCA2 variants and mutants were stained with the 2N antibody. Cells were imaged on a spinning disk confocal microscope (Ultraview; Perkin–Elmer) by using a ×60 oil-immersion objective at a 1.4 N.A. (PlanApo; Nikon, Tokyo, Japan). Regions of interest were selected by applying an edge-finding (Sobel) digital filter, thus limiting the analysis to plasma membrane areas. The total fluorescence intensity in membrane-delimiting regions of interest was quantified with software developed in our laboratory. For each construct, fluorescence was averaged over a total of 50 cells in three different slides.

Ca^{2+} Measurements with Recombinant Aequorin. Transfected cytAEQ was reconstituted by incubating CHO cells for 1–3 h with 5 μM coelenterazine in DMEM supplemented with 1% FCS at 37°C in a 5% CO$_2$ atmosphere. Additions to the KRB medium (1 mM CaCl$_2$/100 μM ATP) were made as specified in the figure legends. The experiments were terminated by lysing the cells with 100 μM digitonin in a hypotonic Ca^{2+}-rich solution (10 mM CaCl$_2$ in H$_2$O) to discharge the remaining aequorin pool. Briefly, a 13-mm round coverslip with the transfected cells was placed in a perfused thermostated chamber in close proximity to a low-noise photomultiplier, with a built-in amplifier discriminator. The output of the discriminator was captured by a Thorn-EMI photon-counting board and stored in an IBM-compatible computer for further analyses. Luminescence was calibrated off-line into [Ca^{2+}] values by using a computer algorithm based on the Ca^{2+} response curve of WT aequorin (36).

Data are reported as means ± SD. Statistical differences were evaluated by Student's two-tailed t test for unpaired samples. A P value of <0.01 was considered statistically significant.

Organotypic Cultures of Utricles and Cochleae. Sensory epithelia of utricle or cochleae were excised from PMCA2 KO, dfw, or WT mice. Organs were dissected from mice between P1 and P4. The care and use of the animals were approved by the Animal Care and Use Committee of the University of Padua. The otic capsule was opened medially, and the endolymphatic compartment of the utricle was cut open. The otolithic membrane was removed after 15 min of incubation in dissection saline to which 0.1 g/liter bacterial subtilisin protease (type XXIV; Sigma–Aldrich, St. Louis, MO) had been added. Dissection saline was composed of Hank's balanced salt solution (HBSS, catalog no. H6648; Sigma–Aldrich) with 10 mM Hepes, 10.000 units/liter penicillin and 25 μg/liter fungizone. HBSS contained 0.4 g/liter KCl, 0.06 g/liter KH$_2$PO$_4$ (anhydrous), 0.35 g/liter NaHCO$_3$, 8.0 g/liter NaCl, 0.048 g/liter Na$_2$HPO$_4$ (anhydrous), and 1 g/liter D-glucose. The cultures were preserved for 1 day at 37°C in a complete medium of 95% DMEM/Ham's F-12 (1:1) (1×, liquid, with L-glutamine, without Hepes; GIBCO, Carlsbad, CA) and 5% FBS.

Fluorescence Imaging and UV Photolysis of Caged Ca^{2+}. To obtain images of the hair cell along its main axis, the utricle epithelium was fixed at culture time by Cell-Tak (mixed to 90% NaHCO$_3$; BD Biosciences, Bedford, MA) to the lateral side of a glass ball ($\approx$2 mm in diameter) that was previously glued to a microscope slide by a small drop of Sylgard Silicon Elastomer (Dow Corning, Wiesbaden, Germany). At recording time, cultures were loaded with 10 μM cell-permeant Fluo-4 for 50 min at 37°C in DMEM (Invitrogen) supplemented with 10 μM cell-permeant o-nitrophenyl-EGTA AM (Invitrogen), 25 μM sulfinpyrazone and Pluronic F-127 (0.1% wt/vol). For deesterification, cultures were transferred to a chamber mounted on the stage of a confocal imaging setup [a Radiance 2100 (Bio-Rad, Hercules, CA) incorporating a Nikon Eclipse E600FN microscope] and superfused for 20 min with a medium composed of HBSS supplemented with 4.4 g/liter glucose and 2 mM anhydrous CaCl$_2$ (pH 7.4, Osm 330). Experiments were performed with a ×100 water-immersion objective with a N.A. of 1.00 (LUMPlanFl; Olympus, Tokyo, Japan). Fluo-4 fluorescence was excited by the 488-nm line of an argon laser coupled by fiber optics to the microscope. Fluorescence emission was selected $\approx$528 nm by using a narrow-band interference filter (D528/50m; Chroma Technology, Brattleboro, VT). A rapid increase in cytosolic Ca^{2+} was achieved by photorelease of Ca^{2+} from the caged state (o-nitrophenyl-EGTA bound to Ca^{2+}). The UV illumination for uncaging covered an area of $\approx$5,000 μm^2, comprising a few hair cells, and was generated by a 375-nm laser (an LCDU12/7342 at a maximum power of 8 mW; Power Technology, Little Rock, AR) connected to the microscope through a 600-μm-diameter optical fiber. Fiber output was placed in the focal plane of a UV-

transparent positive lens, and the recollimated light beam was reflected off of a 400 DCLP dichromatic beam splitter (Chroma) positioned at 45° just above the microscope objective lens. UV light, controlled by a transistor–transistor logic signal generated by the Bio-Rad 2100 at the end of each frame, was delivered for 50–100 ms during the scanning pause (≈1 s) between the 15th and 16th frames. Images were acquired with a resolution of 512 × 512 pixels by scanning at 512 lines per second under control of Bio-Rad Laser Sharp software. All data were analyzed offline on a personal computer with the Matlab 7.0 (MathWorks, Natick, MA) software environment.

Mechanical Stimulation of Hair Cells. Experiments were performed on OHC of the first row of the mid-apical turn of the organ of Corti. Bundles were deflected with a stiff glass pipette mounted on a piezoelectric bimorph with submillisecond rise times (10–90%) in response to prefiltered (1 kHz) square command steps supplied by the A/D-D/A interface (Digidata 1322; Axon Instruments, Foster City, CA). The tip of the pipette was fire-polished to fit the V-shape of the hair cell stereocilia bundle.

Electrophysiological Recordings on Hair Cells. The sensory epithelium was transferred to an experimental chamber placed on the stage of an upright microscope (Olympus BX51W) equipped with differential interference contrast optics and viewed with the LumPlanFL ×100 water objective. Extracellular solutions were continuously superfused at 5 ml/min with a medium containing 144 mM NaCl, 0.7 mM NaH$_2$PO4, 5.8 mM KCl, 1.3 mM CaCl$_2$, 0.9 mM MgCl$_2$, 5.6 mM D-glucose, and 10 mM Hepes-NaOH (adjusted to pH 7.4). The recording pipettes contained a standard intracellular solution that included 140 mM KCl, 0.5 mM EGTA-KOH, 3.5 mM MgCl$_2$, 2.5 mM MgATP, and 5 mM Hepes-KOH (pH 7.4). The recording pipettes were pulled with resistances of 3–5 MΩ from R-6 soda lime glass (Garner Glass, Claremont, CA) and had series resistance of 8–12 MΩ when sealed to cells. Recordings were made from hair cells in the intact epithelium in the whole-cell, tight-seal mode of the patch-clamp technique by using an Axopatch 200B patch-clamp amplifier (Axon Instruments). Transduction (MET) currents were recorded from cells held at −80 mV, filtered at 1 kHz with an 8-pole Bessel filter (Axon Instruments), digitized at 4 kHz with a 12-bit acquisition board (Digidata 1322) and pClamp 9.2 software (both from Axon Instruments), and stored on a hard disk.

1. Fuchs PA (2005) *J Physiol* 566:7–12.
2. Lim DJ (1986) *Hear Res* 22:117–146.
3. Fettiplace R, Hackney CM (2006) *Nat Rev Neurosci* 7:19–29.
4. Corey DP, Sotomayor M (2004) *Nature* 428:901–903.
5. Anniko M, Wroblewski R (1986) *Hear Res* 22:279–293.
6. Corey DP, Hudspeth AJ (1979) *Nature* 281:675–677.
7. Ohmori H (1985) *J Physiol* 359:189–217.
8. Lumpkin EA, Marquis RE, Hudspeth AJ (1997) *Proc Natl Acad Sci USA* 94:10997–11002.
9. Denk W, Holt JR, Shepherd GM, Corey DP (1995) *Neuron* 15:1311–1321.
10. Jorgensen F, Kroese AB (1995) *Acta Physiol Scand* 155:363–376.
11. Bosher SK, Warren RL (1978) *Nature* 273:377–378.
12. Wood JD, Muchinsky SJ, Filoteo AG, Penniston JT, Tempel BL (2004) *J Assoc Res Otolaryngol* 5:99–110.
13. Corey DP, Hudspeth AJ (1983) *J Neurosci* 3:962–976.
14. Marquis RE, Hudspeth AJ (1997) *Proc Natl Acad Sci USA* 94:11923–11928.
15. Ricci AJ, Fettiplace R (1998) *J Physiol* 506:159–173.
16. Hackney CM, Mahendrasingam S, Penn A, Fettiplace R (2005) *J Neurosci* 25:7867–7875.
17. Ricci AJ, Wu YC, Fettiplace R (1998) *J Neurosci* 18:8261–8277.
18. Lumpkin EA, Hudspeth AJ (1998) *J Neurosci* 18:6300–6318.
19. Yamoah EN, Lumpkin EA, Dumont RA, Smith PJ, Hudspeth AJ, Gillespie PG (1998) *J Neurosci* 18:610–624.
20. Crouch JJ, Schulte BA (1995) *Hear Res* 92:112–119.
21. Wu YC, Tucker T, Fettiplace R (1996) *Biophys J* 71:2256–2275.
22. Shah DM, Freeman DM, Weiss TF (1995) *Hear Res* 87:187–207.
23. Kozel PJ, Friedman RA, Erway LC, Yamoah EN, Liu LH, Riddle T, Duffy JJ, Doetschman T, Miller ML, Cardell EL, Shull GE (1998) *J Biol Chem* 273:18693–18696.
24. Carafoli E, Santella L, Branca D, Brini M (2001) *Crit Rev Biochem Mol Biol* 36:107–260.
25. Guerini D, Coletto L, Carafoli E (2005) *Cell Calcium* 38:281–289.
26. Brodin P, Falchetto R, Vorherr T, Carafoli E (1992) *Eur J Biochem* 204:939–946.
27. Elwess NL, Filoteo AG, Enyedi A, Penniston JT (1997) *J Biol Chem* 272:17981–17986.
28. Niggli V, Adunyah ES, Penniston JT, Carafoli E (1981) *J Biol Chem* 256:395–401.
29. Crouch JJ, Schulte BA (1996) *Hear Res* 101:55–61.
30. Dumont RA, Lins U, Filoteo AG, Penniston JT, Kachar B, Gillespie PG (2001) *J Neurosci* 21:5066–5078.
31. Hill JK, Williams DE, LeMasurier M, Dumont RA, Strehler EE, Gillespie PG (2006) *J Neurosci* 26:6172–6180.
32. Brini M, Coletto L, Pierobon N, Kraev N, Guerini D, Carafoli E (2003) *J Biol Chem* 278:24500–24508.
33. Street VA, McKee-Johnson JW, Fonseca RC, Tempel BL, Noben-Trauth K (1998) *Nat Genet* 19:390–394.
34. Schultz JM, Yang Y, Caride AJ, Filoteo AG, Penheiter AR, Lagziel A, Morell RJ, Mohiddin SA, Fananapazir L, Madeo AC, Penniston JT, Griffith AJ (2005) *N Engl J Med* 352:1557–1564.
35. Brini M, Bano D, Manni S, Rizzuto R, Carafoli E (2000) *EMBO J* 19:4926–4935.
36. Brini M, Marsault R, Bastianutto C, Alvarez J, Pozzan T, Rizzuto R (1995) *J Biol Chem* 270:9896–9903.
37. Fettiplace R, Ricci AJ (2006) in *Vertebrate Hair Cells*, eds Eatock RA, Fay RR, Popper AN (Springer, New York), Vol 27, pp 154–203.
38. Beurg M, Evans MG, Hackney CM, Fettiplace R (2006) *J Neurosci* 26:10992–11000.
39. Tucker T, Fettiplace R (1995) *Neuron* 15:1323–1335.
40. Wu YC, Ricci AJ, Fettiplace R (1999) *J Neurophysiol* 82:2171–2181.
41. Petit C (2006) *Trends Mol Med* 12:57–64.
42. Hilfiker H, Guerini D, Carafoli E (1994) *J Biol Chem* 269:26178–26183.
43. Assad JA, Shepherd GM, Corey DP (1991) *Neuron* 7:985–994.
44. Gillespie PG, Cyr JL (2004) *Annu Rev Physiol* 66:521–545.
45. Fettiplace R, Ricci AJ (2003) *Curr Opin Neurobiol* 13:446–451.
46. Assad JA, Hacohen N, Corey DP (1989) *Proc Natl Acad Sci USA* 86:2918–2922.
47. Eatock RA, Corey DP, Hudspeth AJ (1987) *J Neurosci* 7:2821–2836.
48. Zhao Y, Yamoah EN, Gillespie PG (1996) *Proc Natl Acad Sci USA* 93:15469–15474.
49. Walker RG, Hudspeth AJ, Gillespie PG (1993) *Proc Natl Acad Sci USA* 90:2807–2811.
50. Boeda B, El-Amraoui A, Bahloul A, Goodyear R, Daviet L, Blanchard S, Perfettini I, Fath KR, Shorte S, Reiners J, *et al.* (2002) *EMBO J* 21:6689–6699.
51. Ricci AJ, Crawford AC, Fettiplace R (2003) *Neuron* 40:983–990.
52. Rizzuto R, Brini M, Bastianutto C, Marsault R, Pozzan T (1995) *Methods Enzymol* 260:417–428.

BIOCHEMISTRY